



Covalently grafted human serum albumin coating mitigates the foreign body response against silicone implants in mice

Xianchi Zhou^{a,1}, Hongye Hao^{a,c,1}, Yifeng Chen^{a,c}, Wenzhong Cao^a, Zihao Zhu^a, Yanwen Ni^a, Zuolong Liu^a, Fan Jia^b, Youxiang Wang^{a,**}, Jian Ji^{a,c,d,*}, Peng Zhang^{a,c,d,***}

^a MOE Key Laboratory of Macromolecule Synthesis and Functionalization of Ministry of Education, Department of Polymer Science and Engineering, Zhejiang University, Hangzhou, PR China

^b Key Laboratory of Cardiovascular Intervention and Regenerative Medicine of Zhejiang Province, Department of Cardiology, Sir Run Run Shaw Hospital, School of Medicine, Zhejiang University, Hangzhou, PR China

^c International Research Center for X Polymers, International Campus, Zhejiang University, Haining, PR China

^d State Key Laboratory of Transvascular Implantation Devices, Zhejiang University, Hangzhou, PR China

ARTICLE INFO

Keywords:

Foreign body response
Implant
Surface coating
Inflammation

ABSTRACT

Implantable biomaterials and biosensors are integral components of modern medical systems but often encounter hindrances due to the foreign body response (FBR). Herein, we report an albumin coating strategy aimed at addressing this challenge. Using a facile and scalable silane coupling strategy, human serum albumin (HSA) is covalently grafted to the surface of polydimethylsiloxane (PDMS) implants. This covalently grafted albumin coating remains stable and resistant to displacement by other proteins. Notably, the PDMS with covalently grafted HSA strongly resists the fibrotic capsule formation following a 180-day subcutaneous implantation in C57BL/6 mice. Furthermore, the albumin coating led to reduced recruitment of macrophages and triggered a mild immune activation pattern. Exploration of albumin coatings sourced from various mammalian species has shown that only HSA exhibited a promising anti-FBR effect. The albumin coating method reported here holds the potential to improve and extend the function of silicone-based implants by mitigating the host responses to subcutaneously implanted biomaterials.

1. Introduction

Implantable biomaterials and biosensors play a pivotal role in contemporary medical systems, yet their functionality and long-term stability are significantly impeded by the foreign body response (FBR) elicited upon implantation [1–6]. The use of synthetic materials like polydimethylsiloxane (PDMS) in clinically used medical devices such as breast implants, cardiac pacemaker, and cochlear implant, can induce varying levels of immune-mediated FBR, leading to the formation of a dense fibrous capsule around the implant [7–13]. While the

administration of anti-inflammatory drugs like glucocorticoid dexamethasone can effectively suppress fibrosis, its effect is short-lived [14–16]. An alternative approach lies in the physical and molecular design of materials, which serve as a promising strategy to mitigate the immune response to implants. Notably, physical properties, including size [17], geometry [18], roughness [19], porosity [20], mechanical properties [21,22], and surface chemistry [23–26], have all demonstrated their influence on immune activation.

Another approach to evade immune system recognition involves mimicking the body's own components. Notably, cell surface markers

Peer review under responsibility of KeAi Communications Co., Ltd.

* Corresponding author. MOE Key Laboratory of Macromolecule Synthesis and Functionalization of Ministry of Education, Department of Polymer Science and Engineering, Zhejiang University, Hangzhou, PR China.

** Corresponding author. MOE Key Laboratory of Macromolecule Synthesis and Functionalization of Ministry of Education, Department of Polymer Science and Engineering, Zhejiang University, Hangzhou, PR China.

*** Corresponding author. MOE Key Laboratory of Macromolecule Synthesis and Functionalization of Ministry of Education, Department of Polymer Science and Engineering, Zhejiang University, Hangzhou, PR China.

E-mail addresses: yx_wang@zju.edu.cn (Y. Wang), jijian@zju.edu.cn (J. Ji), zhangp7@zju.edu.cn (Peng Zhang).

¹ These authors contributed equally: Xianchi Zhou, Hongye Hao.

<https://doi.org/10.1016/j.bioactmat.2024.01.006>

Received 14 August 2023; Received in revised form 3 January 2024; Accepted 5 January 2024

2452-199X/© 2024 The Authors. Publishing services by Elsevier B.V. on behalf of KeAi Communications Co. Ltd. This is an open access article under the CC BY-NC-ND license (<http://creativecommons.org/licenses/by-nc-nd/4.0/>).

such as CD47 and CD200, which act as self-signaling molecules, have shown the ability to diminish immune recognition. The conjugation of material surfaces with CD47 or CD200 has been demonstrated to reduce macrophage activation effectively, but their effect on long-term fibrotic capsule formation has not been reported [27,28]. Additionally, biomaterials derived from natural mucin glycoproteins have shown ability to inhibit immune cascades and evade foreign body responses [29,30]. For example, mucin-based hydrogels have demonstrated resistance to the FBR for a duration of 21 days in mice [31].

Albumin, the most abundant protein in plasma, has been extensively studied for its biomedical applications [32–35]. For instance, bovine serum albumin (BSA) is widely acknowledged for its ability to resist nonspecific protein adsorption, making it a commonly utilized passivating agent in enzyme-linked immunosorbent assays (ELISA) and related experiments to prevent the nonspecific adsorption of other protein molecules. Various methods, including physical adsorption [36], dopamine-conjugated BSA [37], and reductant-induced fast amyloid-like BSA aggregation [38], can be employed to construct albumin coatings on hydrophobic substrates. Such albumin coatings have exhibited excellent anti-fouling properties, reduced macrophage adhesion, and mitigated inflammatory responses in vivo. However, despite great progress in vitro experiments, no albumin coating has so far been able to effectively reduce FBR caused by long-term implant placement. We speculate that albumin coating might be a simple and effective strategy in reducing the long-term FBR associated with implanted devices, while the coating stability might play a crucial role. From the mechanism of nonspecific protein adsorption, the adsorption of proteins on the material surface follows the Vroman effect, where small and abundant protein molecules first cover the surface and then, over time, proteins with higher affinity for specific surfaces will replace them [39]. From this point of view, the practical application of albumin coatings based on surface adsorption in the physiological environment is challenging as the adsorbed albumin is prone to be displaced by other proteins present in body fluids, leading to coating failure.

Herein, considering the risk of albumin coatings failure due to protein replacement, we aimed to investigate whether a stable albumin coating can reduce FBR induced by hydrophobic implants by developing an a covalently grafted albumin coating. Additionally, we also compared the anti-FBR effects of albumin coatings from different species. Unlike the albumin coating by physical adsorption prepared by simple solution immersion, our method firmly attaches albumin to the surface, reducing the displacement of other proteins in the body environment, with the goal of achieving long-term resistance to fibrosis within the body. Considering the acceptance of albumin from different species by participants in subsequent clinical trials, human serum albumin coatings may have a higher possibility of clinical use to improve the performance of various implantable biomedical devices.

2. Material and methods

2.1. Materials

3-Glycidyloxypropyltrimethoxysilane, Fluorescein isothiocyanate (FITC), and acetic acid were supplied by Aladdin Reagent Co., Ltd. Phosphate buffer solution (PBS) was purchased from Sangon Biotech Co., Ltd. Sulfo-Cyanine 5 succinimidyl ester (Sulfo-Cy5 NHS ester) was supplied by Duofluor Inc. FITC labeled bovine serum fibrinogen (Fg-FITC) was purchased from XI'AN QIYUE biology. PEG-NH₂ (Mw = 2000) was purchased from JINGPI Technology. The silicone elastomer Sylgard 184 was obtained from Dow Corning (catalog no. 3097358–1004). Human serum albumin (catalog no. SRP6182), bovine serum albumin (catalog no. A2153), porcine serum albumin (catalog no. A1830), and rat serum albumin (catalog no. A6272) were purchased from Sigma-Aldrich.

2.2. Preparation of PDMS discs

PDMS substrates were prepared and used as controls, with the ratio of prepolymer and curing agent is 10:1 (wt/wt). The mixture was degassed and poured into plastic dishes at a fixed volume, resulting in a PDMS layer with a thickness of ~1 mm. The PDMS layer was cured at 80 °C for 2 h, peeled, and subsequently cleaned with ethanol and dried. The PDMS sheet was cut into discs with a biophysical punch (4 mm in diameter) for the following experiments.

2.3. Fabrication of epoxy group-modified PDMS discs

PDMS discs were cleaned by washing with isopropanol and ethanol and deionized in sequence, followed by drying under nitrogen flow. The cleaned discs were then activated by an oxygen plasma cleaner (30 W at 20 mtorr pressure; Harrick Plasma) for 3 min. After oxygen plasma treatment, the activated discs and 1 g of 3-glycidyloxypropyltrimethoxysilane were put into a vacuum oven, placed at room temperature and left for 12 h. Once the reaction was complete, the discs were washed twice with anhydrous ethanol and DI water, respectively, for 5 min each time. Subsequently, they were washed once more with anhydrous ethanol and then dried in an oven at 60 °C for 1 h.

2.4. Fabrication of covalently grafted/physically adsorbed albumin PDMS discs

The human serum albumin (HSA) solution was prepared by dissolving 10 mg/mL of human serum albumin (HSA) and 0.2 vol% acetic acid in PBS buffer. The epoxy saline coupling agent-treated discs were subsequently immersed in this solution and incubated at 37 °C for 12 h. After incubation, the discs were washed under ultrasonication for 2 min in PBS solution to removes any unbonded albumin from the surface, leaving only covalently bonded albumin on the surface. The resulting sample is denoted as HSA-PDMS. The albumin coating through physical adsorption was prepared using a similar procedure. However, in this case, PDMS discs without the epoxy saline coupling agent treatment were used and washed with or without ultrasound, respectively. Samples grafted with PEG on the surface of PDMS discs were also prepared for comparison. After undergoing the same epoxy group grafting as above, PEG-NH₂ was used instead of albumin for incubation.

2.5. X-ray photoelectron spectroscopy (XPS)

XPS data was obtained with a Thermo Scientific ESCALAB 250Xi spectrometer equipped with an Al K α X-ray source (1486.6 eV). All spectra were collected at a takeoff angle of 30° to the sample surface.

2.6. Contact-angle measurements

The contact angle was measured on the surface of the samples using a contact-angle goniometer (Dataphysics OCA 20) in the air at room temperature. The samples in the PBS were rinsed with water and dried with argon flow. The static contact angles were measured by dispensing a small water droplet of 1.2 μ L on the sample surfaces. The contact angle data were collected from the average of four measurements for each sample.

2.7. Albumin content on disc surface tested by enzyme-linked immunosorbent assay (ELISA)

A Human Serum Albumin ELISA Kit provided by Abclonal (Catalog No. RK00157) was employed to assess the human serum albumin content on the surfaces of HSA-PDMS and HSA+PDMS discs, both before and after implantation. In brief, 4 mm diameter discs were placed in 96-well plates pre-coated with capture antibody and incubated for 2 h, followed by 6 washes with wash buffer. The detection antibody was then

added to plates and incubated for 1 h, followed by 6 washes with wash buffer. Finally, the 3, 3', 5, 5'-tetramethylbenzidine (TMB) chromogen solution was then added to plates. After 15 min incubation, the enzymatic reaction was stopped by adding an equal volume of 2 N H₂SO₄. Absorbance values at 450 nm and 570 nm (as calibration wavelength) were recorded by a microplate reader (MODEL 550, Bio-Rad). Average data were acquired from three specimens.

For *ex vivo* samples, HSA-PDMS and HSA+PDMS discs were implanted in C57BL/6 mice for 1 month, after which the samples were explanted. The HSA-PDMS discs were manually separated from the tissue and subsequently subjected to ultrasonic cleaning in water containing detergent for a duration of 5 min. Then rinsed HSA-PDMS and HSA+PDMS discs with deionized water. The samples underwent ELISA testing using the same method as described above.

2.8. Fibrinogen displacement test

The stability of human serum albumin coatings prepared by different methods was examined using a fibrinogen displacement test. Firstly, the coating samples were incubated with Sulfo-Cy5 NHS ester (100 µg/mL) under room temperature, which labeled the amino groups on the albumin, followed by rinsing with deionized water. Then, the samples were incubated with Fg-FITC (1 mg/mL) under room temperature for 24 h to facilitate protein replacement and subsequently rinsed again. Finally, fluorescent images of each step were acquired using a scanning confocal system (Zeiss LSM 780).

2.9. Ellipsometry

For ellipsometry test, HSA was coated on silica substrates following the same approach as described above. The thickness of albumin coating was measured by a spectroscopic ellipsometer (M – 2000, J. A. Woolam).

2.10. Fluorescence labeling of albumin coating

Coating samples were labeled using FITC to confirm successful grafting or adsorption of albumin on PDMS. Albumin-grafted samples were soaked in FITC aqueous solution (10 µg/mL) for 30 min and rinsed in PBS before the test. The fluorescent images were captured by a Nikon DS-Ri2 microscope.

2.11. Animal work

All animal experiments are in compliance with the relevant regulations, and all protocols are approved by the Animal Care and Use Committee, Zhejiang Academy of Medical Sciences. Wild-type (WT) female C57BL/6 mice of 6–8 weeks of age were obtained from the animal center of Zhejiang Academy of Medical Sciences. The animals were fed a standard laboratory diet and maintained with a 12-h light/12-h dark cycle.

For procedures in mice, discs were sterilized by ultraviolet irradiation and implanted subcutaneously in C57BL/6 female mice. The implantation procedure was as follows. In brief, mice were anaesthetized with 3% isoflurane in oxygen, shaved, and disinfected the skin with iodine. About 8 mm longitudinal incision was made on the dorsal surface, using surgical scissors to provide access to the subcutaneous space. Then subcutaneous pockets about 0.5 cm away from the incision were created with blunt forceps for the implantation of the elastomer discs. After implantation, the incisions were closed using 5–0 taper-tipped PGA absorbable sutures. Mice were monitored until recovery from anesthesia and raised for 1 day, 2 weeks, and 4 weeks, respectively. The mice grew normally with no sign of discomfort after the implantation, and no body weight loss was observed before explantation. The mock group without surgery was used as control.

2.12. Retrieval of tissues and elastomers

After 1 day, 5 days, 2 weeks, and 4 weeks, 12 weeks, and 24 weeks respectively, mice were sacrificed and the implants together with the surrounding tissue were excised and collected. The explanted samples were either fixed in 10% formaldehyde solution (for use in histology) or flash-frozen (for RNA analysis).

2.13. Immunostaining of tissue sections, microscopy and quantitative image analysis

Paraformaldehyde-fixed tissue samples were dehydrated in graded ethanol series and embedded in paraffin. Sections with a thickness of 3–5 µm were cut using a microtome, deparaffinized in xylene and rehydrated in sequential baths of ethanol: distilled water. Sections were further stained with haematoxylin and eosin (cellularity) and Masson's trichrome (collagen) according to standard histological protocols. For immunohistochemistry, heat-induced epitope retrieval with 0.1 M citrate buffer (pH 6) was performed for 15 min at 95 °C and sections were further rehydrated by three washes in PBS with 0.1% Tween wash buffer. Immunohistochemical staining was performed according to the manufacturer's instructions (Diaminobenzidine (DAB) chromogenic reagent kit; DAKO; catalog no. K5007). Briefly, sections were blocked with peroxidase blocking solution for 10 min at room temperature, followed by three washes in PBS with 0.1% Tween wash buffer. Primary antibodies directed against CCR-7 (rabbit IgG; dilution 1:500; Abcam; catalog no. ab253187), TNF-α (goat IgG; dilution 15 µg/mL; R&D systems; catalog no. AF-410), and IL-6 (goat IgG; dilution 15 µg/mL; R&D systems; catalog no. AF-406) were used. This step was followed by incubation with anti-rabbit or anti-goat secondary horseradish peroxidase-conjugated antibodies goat anti-rabbit IgG (HRP polymer; SE134; Solarbio) and rabbit anti-goat IgG (HRP polymer; GB23204; Servicebio). For immunofluorescence staining, tissue sections were incubated in 0.1 M citrate buffer (pH 6) for 15 min at 95 °C and afterward rehydrated by three washes in TBS + 0.025% Triton X-100 wash buffer. Sections were incubated in 10% goat serum for 60 min, followed by overnight incubation with primary antibodies against F4/80 (rabbit IgG; dilution 1:5000; Abcam; catalog no. ab300421), α-SMA (Cy3 polymer; mouse IgG2a; dilution 3 µg/mL; Sigma; catalog no. C6198), CD3 (Brilliant Violet 421 polymer; rat IgG2b; dilution 3 µg/mL; BioLegend; catalog no. 100228), and F4/80 (Alexa Fluor 647 polymer; rat IgG2a; dilution 5 µg/mL; BioLegend; catalog no. 123122). The isotype-specific secondary antibody Alexa Fluor® 488-conjugated goat anti-rabbit IgG (H + L) F(ab')₂ Fragment (dilution 1:200; catalog no. 4412 S; Cell Signaling Technology) was used to detect primary antibodies. 4',6-diamidino-2-phenylindole (DAPI) dihydrochloride (1:50; D9542; Sigma-Aldrich) was used to visualize the nuclei. Images were acquired with a microscope (Nikon intensilight CHGFI) equipped with the NIS-Elements AR software and a Virtual Slide Microscope (VS120-S6-W, Olympus, Japan). The collagen density is measured by the percentage of blue-pixel coverage in the M&T images of tissues within 50 µm (at 10 µm steps) from the material-tissue interface. The density of blue pixels was determined using Photoshop software. Regions positive (OD value) for TNF-α, IL-6, and CCR-7 were collected in the tissue within 50 µm from the tissue-material interface as a percentage of the positive staining in the entire deep or fascia-facing capsule area using ImageJ. All images were processed using Adobe Photoshop 2023 (Adobe Systems). The contrast and brightness were enhanced consistently for all representative images used. Only one piece of the corresponding sample of each group was implanted into each mouse.

2.14. RNA-seq and data analysis

All appliances used were treated with diethyl pyrocarbonate (DEPC) for RNA-DNase free before the experiment. After implantation of discs, tissue samples surrounding implant materials were excised and

immersed into RNA-later solution from Sigma-Aldrich (catalog no. R0901) to preserve, using a mock group without implantation as control. RNA samples were qualified and quantified using a NanoDrop and Agilent 2100 bioanalyzer (Thermo Fisher Scientific, MA, USA). The RNA sequencing libraries were constructed and sequenced on the BGISEQ-500 platforms. The data with a P value less than 0.05 with a significant difference between the PDMS and HSA-PDMS group data were counted. The mock group without implantation was used as control. The RNA-seq data were collected from the average of three mice for each sample.

2.15. Quantitative PCR assay

Total RNA was extracted from skin tissue near the material by using TRIzol reagent and RNase-Free DNase Set (Qiagen). qRT-PCR was conducted by using Power SYBR Green Master Mix (Applied Biosystems) according to the manufacturer's instructions. The extracted and purified RNA samples (500 ng) were reverse transcribed into complementary DNA (cDNA) using a SuperScript™ III First-Strand Synthesis SuperMix (Thermo Fisher). The qRT-PCRs were performed on the Real-Time PCR Detection Systems (CFX384, Bio-Rad, USA) using the manufacturer's recommended settings for quantitative and relative expression. Primers used for qRT-PCR are listed in [Supplementary Table 1](#). The mock group

without implantation was used as control. The PCR data were collected from the average of eight mice for each sample.

2.16. Statistical analysis

Details of the sample size and appropriate statistical test are included in the figure captions. The data are expressed as means \pm s.d. The data were analyzed for statistical significance by one-way analysis of variance (ANOVA) with Turkey post-test using SPSS Statistics 26.0.

3. Results

3.1. Fabrication and characterization of albumin coating

In this study, we developed a covalently grafted albumin coating on the PDMS substrate, designated as HSA-PDMS, through a three-step process involving plasma treatment of the substrate, reaction with the silane coupling agent, and subsequent incubation with the albumin solution. For comparative purposes, samples prepared using a straightforward physical adsorption technique were also prepared and denoted as HSA+PDMS ([Fig. 1a](#)). The successful coating of albumin was confirmed by the emergence of the N 1s peak, along with the C=O and C–O/C–N peaks in XPS ([Fig. 1b,c](#), [Fig. S1](#)), increased surface

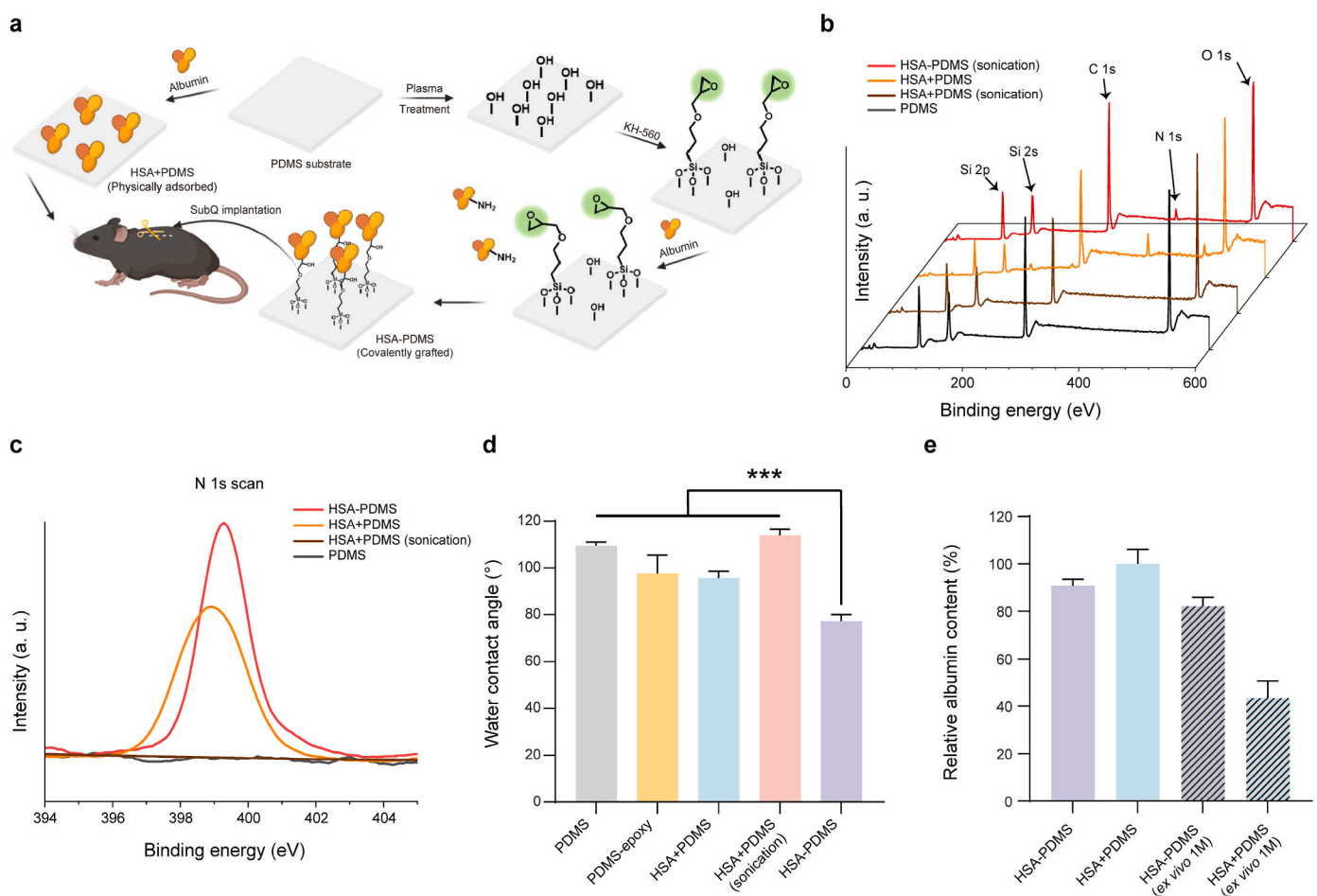


Fig. 1. Preparation and characterization of albumin coating on PDMS substrates. Sample including HSA-PDMS (covalently grafted albumin coating), HSA+PDMS (physically adsorbed albumin coating), HSA-PDMS (sonication) (covalently grafted albumin coating with ultrasound washing for 2 min), HSA + PDMS (sonication) (physically adsorbed albumin coating with ultrasound washing for 2 min), PMDS-epoxy (3-glycidyloxypropyltrimethoxysilane treatment), and PDMS were characterized. **a**) Schematic illustration of the preparation of albumin coating and the subsequent animal works. Figure created with BioRender. **b**) XPS survey spectra of samples. **c**) High-resolution XPS spectra of N 1s for samples. **d**) The water contact angle (WCA) of samples ($n = 5$ samples per group, mean \pm s.d.). **e**) The quantitative measurements of surface albumin. Data were normalized to that of HSA+PDMS sample. Statistical significance was determined by one-way analysis of variance (ANOVA) with Turkey post-test. * $P < 0.05$, ** $P < 0.01$, *** $P < 0.001$, **** $P < 0.0001$, ns: not significant. $P < 0.05$ is considered to have a significant difference.

hydrophilicity observed in WCA test (Fig. 1d), and fluorescence labeling of surface proteins in fluorescent photos (Fig. S2). Of note, the physically adsorbed albumin coating detached from the substrate after 2 min of ultrasonic cleaning, whereas the covalently grafted coating remained, indicating its exceptional stability (Fig. 1b,c, Fig. S1). The preparation of the albumin coating is a straightforward and scalable process, yielding a coating with remarkable stability. Ellipsometry was applied to measure the coating thickness on a silica substrate, which showed a dry thickness

of approximately 3 nm, indicating the formation of a monolayer. The enzyme-linked immunosorbent assay (ELISA) method was employed to quantify the surface albumin grafting density of HSA-PDMS and HSA+PDMS discs. The obtained results reveal comparable albumin grafting densities for samples prepared through both physical adsorption and chemical grafting (Fig. 1e). To assess the *in vivo* stability of the albumin-coated samples, we subcutaneously implanted them in mice for a duration of 1 month before explantation. Following manual disc

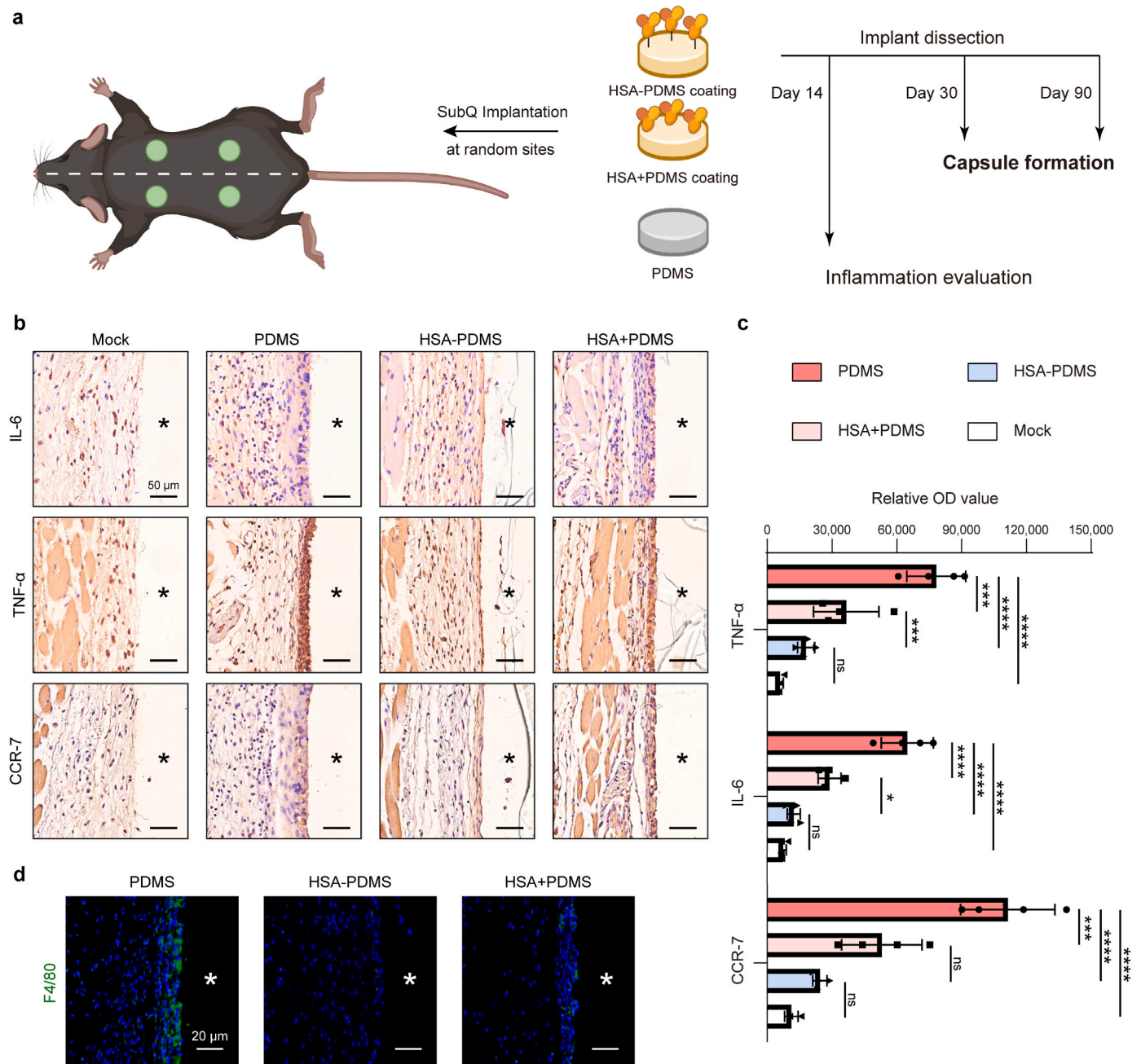


Fig. 2. Assessment of acute inflammatory response induced by the implants. **a)** Discs made of PDMS with and without albumin coating with a diameter of 4 mm and a thickness of 1 mm were implanted subcutaneously (SubQ) on mouse backs. The tissue surrounding the implants were analyzed 14, 30, 90-day post implantation. Immunohistochemistry (IHC) was performed for inflammatory markers (TNF- α , IL-6, and CCR7) (staining shown in **b**), with quantification shown in **c**) 2-week post-implantation. Cells stained by inflammatory markers show brown color, while all nuclei stained with haematoxylin show blue color. Asterisk sign "*" in the section images denote the original locations of the implants. Data were collected in the tissue within 50 μ m from the tissue-material interface ($n = 3$ mice per group, mean \pm s.d.). **d)** Immunofluorescence staining densities of F4/80 (represented by green staining). Counterstaining was performed with DAPI (blue) for cell nuclei. ($n = 3$ mice per group). Asterisk sign "*" in the section images denote the original locations of the implants. Statistical significance was determined by one-way analysis of variance (ANOVA) with Turkey post-test. * $P < 0.05$, ** $P < 0.01$, *** $P < 0.001$, **** $P < 0.0001$, ns: not significant. $P < 0.05$ is considered to have a significant difference.

stripping, ultrasonic cleaning was performed on the HSA-PDMS sample, while the HSA+PDMS sample underwent rinsing. Subsequently, the ELISA test was repeated. The outcomes demonstrate that HSA-PDMS samples retained 86% of the albumin, whereas HSA+PDMS samples only retained 42%. This discrepancy underscores the superior biostability of HSA-PDMS *in vivo*.

3.2. The albumin coating mitigates the acute inflammatory response of implants

Inflammation constitutes a pivotal stage within the FBR cascade, which starts 4–7 days post-implantation, and is characterized by the presence of monocytes and lymphocytes around the implant material. Monocytes infiltrate and undergo differentiation into macrophages which play a vital role in the immune regulation and wound healing process. We investigated the acute inflammatory response induced by the HSA-coated PDMS discs following subcutaneous implantation for five days and two weeks and observed negligible inflammation associated with HSA-PDMS (Fig. 2). Following a five-day implantation period, noticeable cellular deposition and fibrotic reactions were observed on the surfaces of PDMS and HSA+PDMS discs. In contrast, HSA-PDMS discs exhibited minimal changes during the same period (Fig. S3). Immunohistochemical analysis of pro-inflammatory markers, including CCR-7, TNF- α , and IL-6, was performed to assess the impact of albumin-coated PDMS disc implantation on the level of inflammation in the surrounding tissues (Fig. 2b and c). The results indicated that uncoated PDMS exhibits a significant expression in inflammatory markers at the interface between the material and tissue. In contrast, the expression of inflammatory markers is notably lower for discs with albumin coating, with HSA-PDMS demonstrating the most prominent reduction (~1/4 to 1/5 fold of those observed in the tissue surrounding the uncoated PDMS). Macrophages are critical in modulating the inflammatory response and are considered a key cell type in the conventional theory of FBR [40]. Considering their significance, we further investigated the effect of albumin coating on macrophage behavior. Immunofluorescent staining of F4/80 revealed substantial recruitment of macrophages near uncoated PDMS implants, while only a few macrophages were observed near HSA+PDMS implants. In contrast, almost no macrophages were observed around HSA-PDMS implants at 2 weeks (Fig. 2d). The above results indicate that HSA-PDMS induced a negligible inflammatory response after short-term subcutaneous implantation in mice.

3.3. Implants with covalent albumin coating elicit minor immunological and fibrotic responses

The subcutaneous implantation tests were conducted on C57BL/6 mice, with each mouse receiving implants of all three samples on its back. The discs were taken out one month after implantation, and the representative photos and histological images are shown in Fig. 3a. Histological staining (Masson's trichrome and haematoxylin and eosin (H&E)) revealed that HSA-PDMS and HSA+PDMS samples showed ~65% and ~90% collagen density at the interface compared with PDMS discs, respectively (Fig. 3b). This discrepancy indicates a notably diminished FBR. Additionally, we examined the fibrotic response of PDMS treated solely with plasma and determined that plasma treatment did not yield a significant reduction in the fibrotic reaction of PDMS discs. In comparison to PEG-grafted discs, HSA-PDMS discs exhibited markedly superior anti-fibrotic effects (Fig. S4). The recruitment of macrophages, fibroblasts, and T cells on the material-tissue surface after one month of implantation also showed the same trend (Fig. S5). Compared with the large number of FBR-related cell infiltrations on the surface of PDMS control, HSA+PDMS showed a certain degree of cell infiltration, while HSA-PDMS showed almost no cell infiltration. Next, we conducted a quantitative polymerase chain reaction (qPCR) analysis to confirm the difference in the expression of the key factors (Fig. 3c–Table S1). The gene expressions associated with fibrous capsule

formation, such as fibroblast marker alpha-smooth muscle actin (Acta-2) (α -SMA), tissue remodeling marker collagen type I alpha 1 (Col1a1), fibrosis factor interleukin-17 (IL-17), and inflammatory marker tumor necrosis factor alpha (TNF- α) along with interleukin-1 beta (IL-1 β), did not show a significant difference between the tissues surrounding HSA-PDMS and normal tissues, while that around PDMS were all significantly upregulated. From the observations we see that covalently grafted albumin performed significantly better than physically adsorbed albumin, with milder inflammation and capsule formation. Since the nonspecific protein adsorption has been considered the initial step that instigates the FBR once the material has been implanted [3], we speculate that protein displacement may happen to the HSA+PDMS sample due to the Vroman effect. Therefore, we tested the protein displacement behavior of albumin-coated samples using fibrinogen, which is a large blood plasma protein that strongly adsorbs to hydrophobic surfaces. The results showed that after incubation with fibrinogen solution, there was no significant displacement behavior of albumin on the surface of HSA-PDMS, while significant fibrinogen adsorption on the surface of HSA+PDMS and uncoated PDMS was observed (Fig. 3d,e and Fig. S6). Collectively, these data provide strong evidence in favor of utilizing chemical grafting for albumin coating preparation, as opposed to physical adsorption. The chemically grafted coatings demonstrate exceptional stability and resistance to the displacement of other proteins, suggesting the possibility of conferring long-term anti-FBR capabilities to albumin coatings when used *in vivo*.

3.4. RNA-seq of implants with covalent albumin coating

To gain a deeper understanding of the immune response driving the fibrotic response around albumin-coated materials, we performed RNA-sequencing (RNA-seq) on tissues near the implants at 1-month post-implantation, using a mock group without implantation as the control (Fig. 4). Under the condition of $P < 0.05$, the number of differentially expressed genes in the PDMS and mock groups were 2038 while in the HSA-PDMS and mock groups was only 15 (Fig. 4a and b), indicating a minor immune reaction induced by HSA-coated discs. Among the top 10 upregulated genes listed in the table, we found an overall higher expression of the upregulated genes induced by uncoated PDMS compared to HSA-PDMS implants (Fig. 4c). Kyoto Encyclopedia of Genes and Genomes (KEGG) pathway enrichment analysis of the two groups showed that the changed genes in PDMS compared with the mock group were mainly concentrated in FBR-related pathways, such as immune response and regulation of cytokine production, whereas the genes significantly changed in HSA-PDMS compared with mock were not FBR-related (Fig. 4d and e). Gene Ontology (GO) analysis indicate significant disparities in gene expression between HSA-PDMS and PDMS in the immune system process (Fig. S7). We also performed KEGG pathway classification analysis and found that the PDMS/mock comparison generally had a higher number of differential genes than the HSA-PDMS/mock comparison, with 168 and 2 differential genes observed, respectively, in the immune system (Fig. 4f). Notably, the HSA-PDMS implants alleviated the RNA expression of FBR-related tissue remodeling factors (Acta2/ α -SMA, a marker of myofibroblast formation and Mcam/CD146, a marker for endothelial cell lineage), chemokines, and inflammatory response-related cytokines (Fig. 4g). The above results indicate that HSA-PDMS implants induced a significantly weaker immune response than PDMS after subcutaneous implantation in mice.

3.5. Comparing the performance of albumin coatings from various species

Despite sharing significant sequence homology, albumins from different mammalian sources also exhibit variations in their sequences, resulting in immunogenicity across species. For instance, injecting bovine serum albumin (BSA) into rabbits can stimulate humoral immunity to express anti-BSA antibodies [41]. Considering the practical application of medical devices, we selected human serum albumin as the

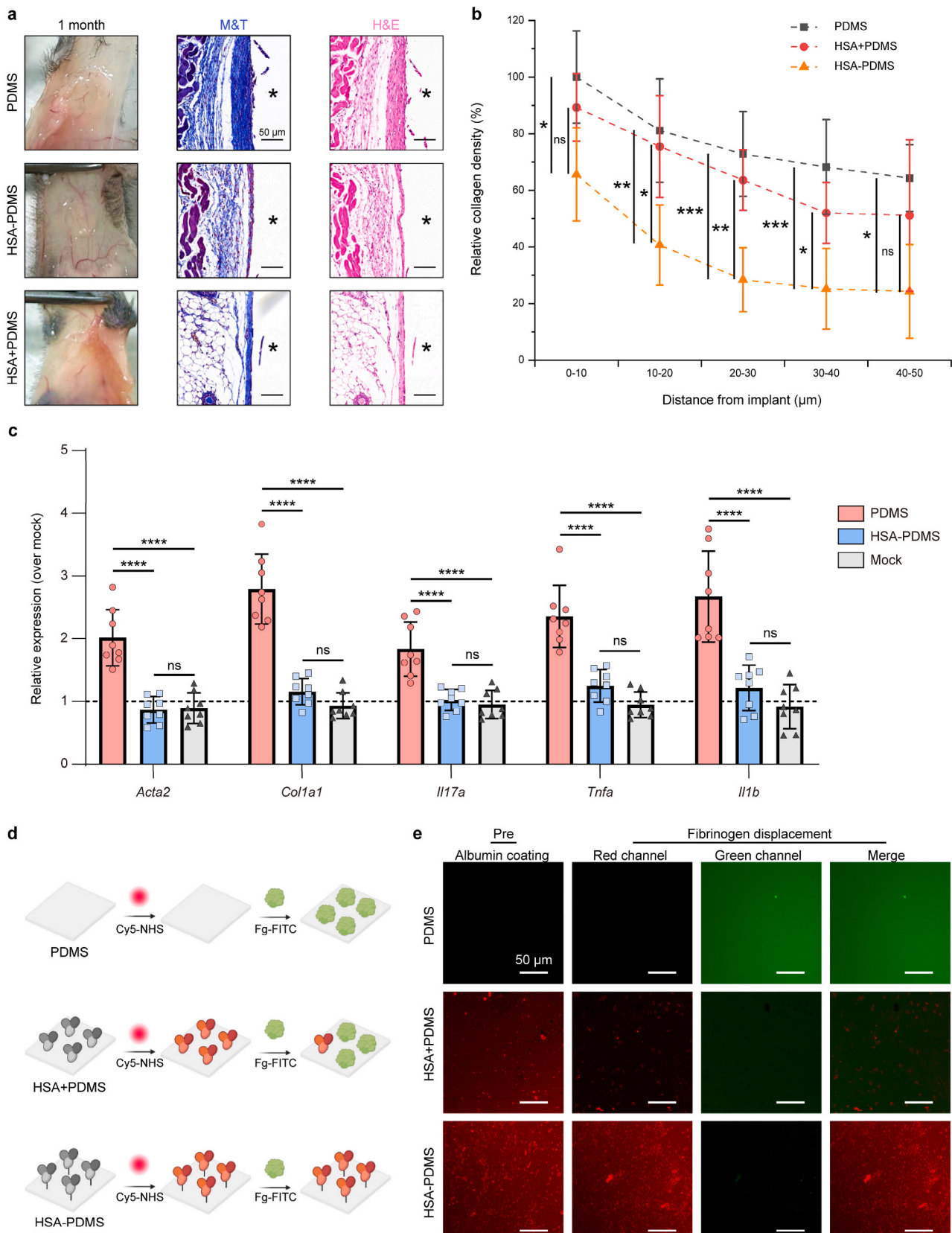


Fig. 3. Anti-fibrotic efficacy and impedance to protein replacement of albumin-coated materials. **a)** Digital photos, H&E-, and M&T-stained histological sections of excised 1-month post-implantation. Asterisk sign "*" in the section images denote the original locations of the implants. **b)** Collagen capsule density 1-month post-implantation measured by M&T staining (n = 6 mice per group, mean ± s.d.). **c)** qRT-PCR analysis of mRNA expression for FBR-related genes. (n = 8 mice per group, mean ± s.d.). **d)** Schematic illustration of the protein replacement experiment. **e)** Fluorescent image of the albumin-coated discs and PDMS control. Albumin on the surface was labeled red and fibrinogen was labeled green. Statistical significance was determined by one-way analysis of variance (ANOVA) with Turkey post-test. **P* < 0.05, ***P* < 0.01, ****P* < 0.001, *****P* < 0.0001, ns: not significant. *P* < 0.05 is considered to have a significant difference.

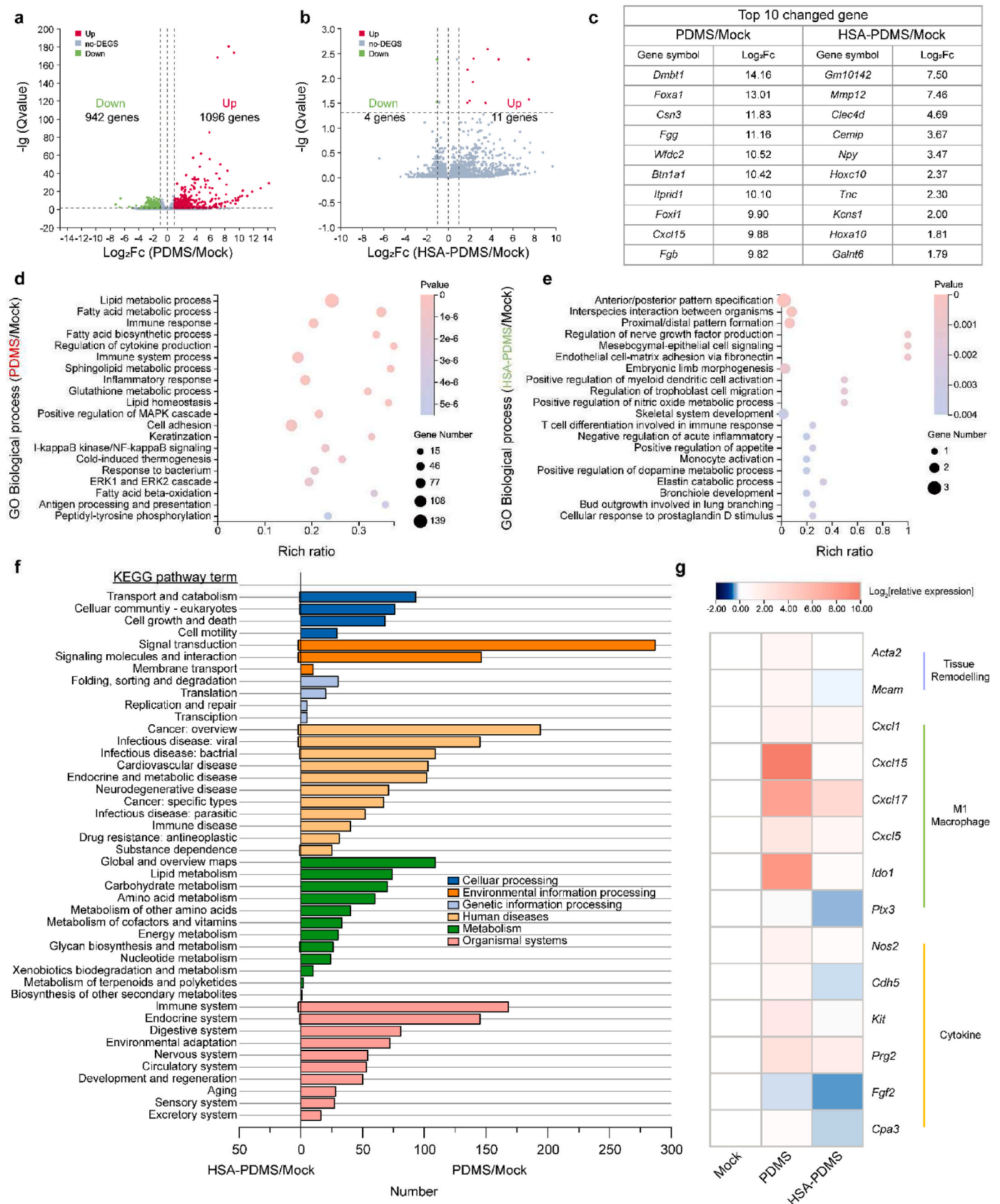


Fig. 4. RNA-seq 1-month post-implantation. **a, b, c)** Significant gene expression changes of PDMS/mock comparison (**a**) and slight changes of HSA-PDMS/mock comparison (**b**) in genes, and a list of top 10 upregulated genes and corresponding log₂Fc (log 2 fold change) (**c**). **d, e, f)** KEGG pathway enrichment analysis of PDMS/mock comparison (**d**) and HSA-PDMS/mock comparison (**e**). **f)** KEGG pathway classification analysis of PDMS/mock comparison and HSA-PDMS/mock comparison. **g)** Gene expression analysis of FBR-related factors in tissues surrounding the PDMS and HSA-PDMS, with data normalized to the mock group (without implantation). n = 3 mice per treatment.

coating material, while it unexpectedly demonstrated minimal FBR in mouse subcutaneous models. Given the substantial sequence homologies found in albumins from various mammals [42], we are wondering whether other mammalian albumin coatings have similar performance to mitigate the FBR of implants in mice. Therefore, we compared the

FBR resistance performance of the albumin coatings sourced from diverse animal origins, including BSA, porcine serum albumin (PSA), and rat serum albumin (RSA), head-to-head with that of the HSA (Fig. 5a). The subcutaneous implantation tests were conducted on C57BL/6 mice with each mouse receiving implants of all samples on its

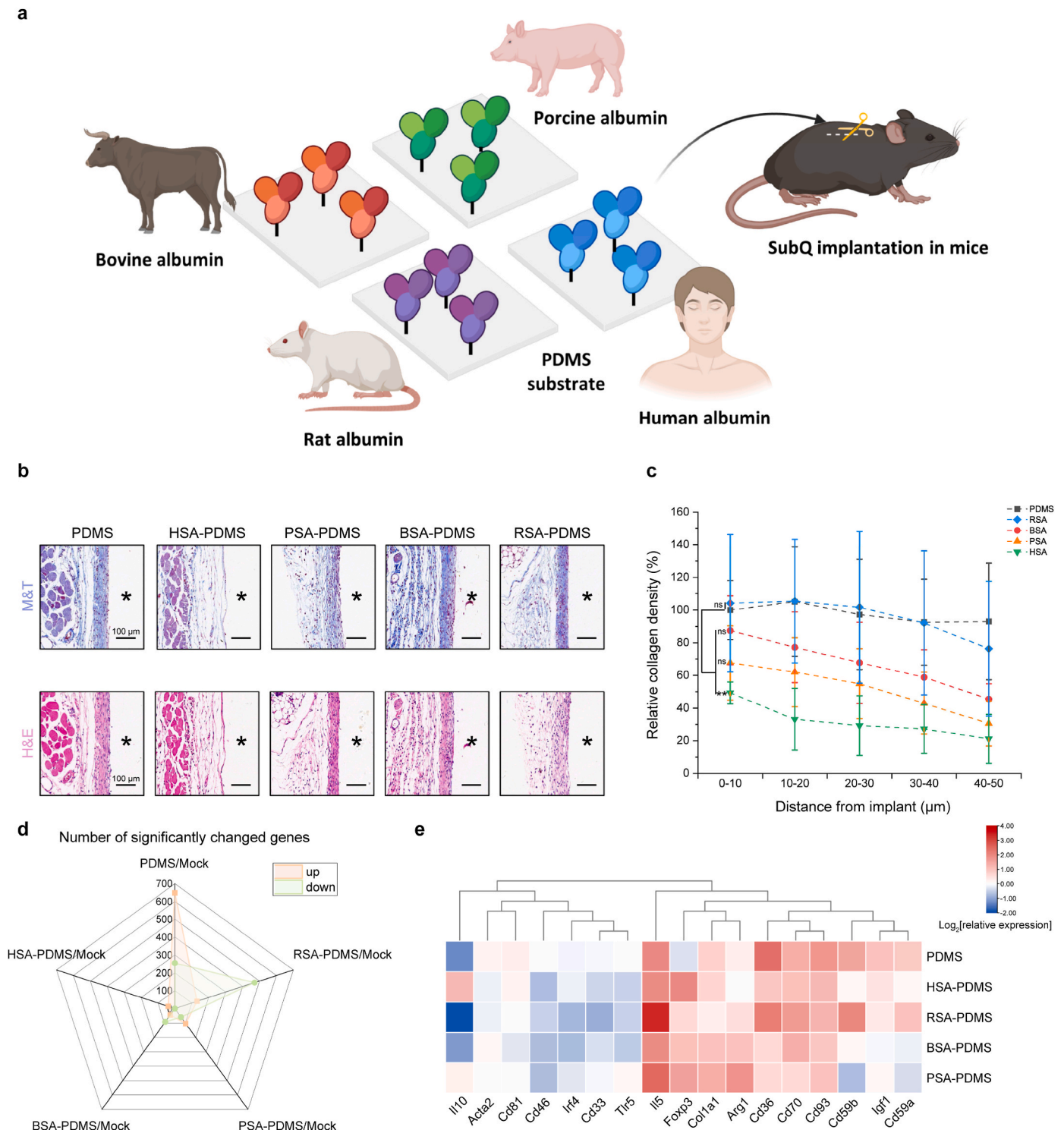


Fig. 5. The performance of albumin coatings from different species. **a)** Schematic illustration of the albumin coatings from different species. **b)** H&E- and Masson’s trichrome (M&T)-stained histological sections of excised tissue 2-week post-implantation. Asterisk sign “*” in the section images denote the original locations of the implants. **c)** Collagen capsule density measured by M&T staining (n = 5 mice per group, mean ± s.d.). **d)** Gene expression changes of albumin coating from different species/Mock after 1-month implantation. **e)** Gene expression analysis of FBR-related factors in tissues surrounding the implants. n = 3 mice per treatment. Statistical significance was determined by one-way analysis of variance (ANOVA) with Turkey post-test. *P < 0.05, **P < 0.01, ***P < 0.001, ****P < 0.0001, ns: not significant. P < 0.05 is considered to have a significant difference.

back. The discs were taken out two weeks after implantation, and the representative photos and histological images are shown in Fig. 5b. Histological staining distinctly underscored the supremacy of human serum albumin coatings compared with other mammalian albumins, showed a reduction of ~50% in collagen density compared to uncoated PDMS (Fig. 5c). Nonetheless, a deeper comprehension of the underlying mechanisms necessitates further investigation. To gather additional insights, an RNA-seq test was conducted across various species. In comparison to the mock group, HSA-PDMS exhibited the fewest differentially expressed genes, with only 39 genes affected, whereas PDMS and RSA-PDMS displayed more substantial genetic alterations, with 903 and 602 affected genes, respectively (Fig. 5d). Examining gene expression patterns, HSA-PDMS samples demonstrated lower expression levels of Acta-2 (a fibroblast marker) and Col1a1 (a fibrosis marker) in

contrast to PDMS. Concurrently, there was an elevation in the expression of anti-inflammatory markers such as Il10 and Foxp3 (Fig. 5e). These findings suggest a distinctive genetic response associated with HSA-PDMS.

3.6. Covalently grafted HSA coating resists long-term FBR

Maintaining long-term resistance to fibrous capsule formation is crucial for the functionality of implantable devices and prosthetics within the body. To assess this, we conducted long-term implantation tests and retrieved the implants after 3 and 6 months for fibrosis analysis. Remarkably, HSA-PDMS discs retained distinct contours and exhibited loose fibrous capsules, as evidenced by digital images and M&T staining (Fig. 6a and c). In stark contrast, the uncoated PDMS

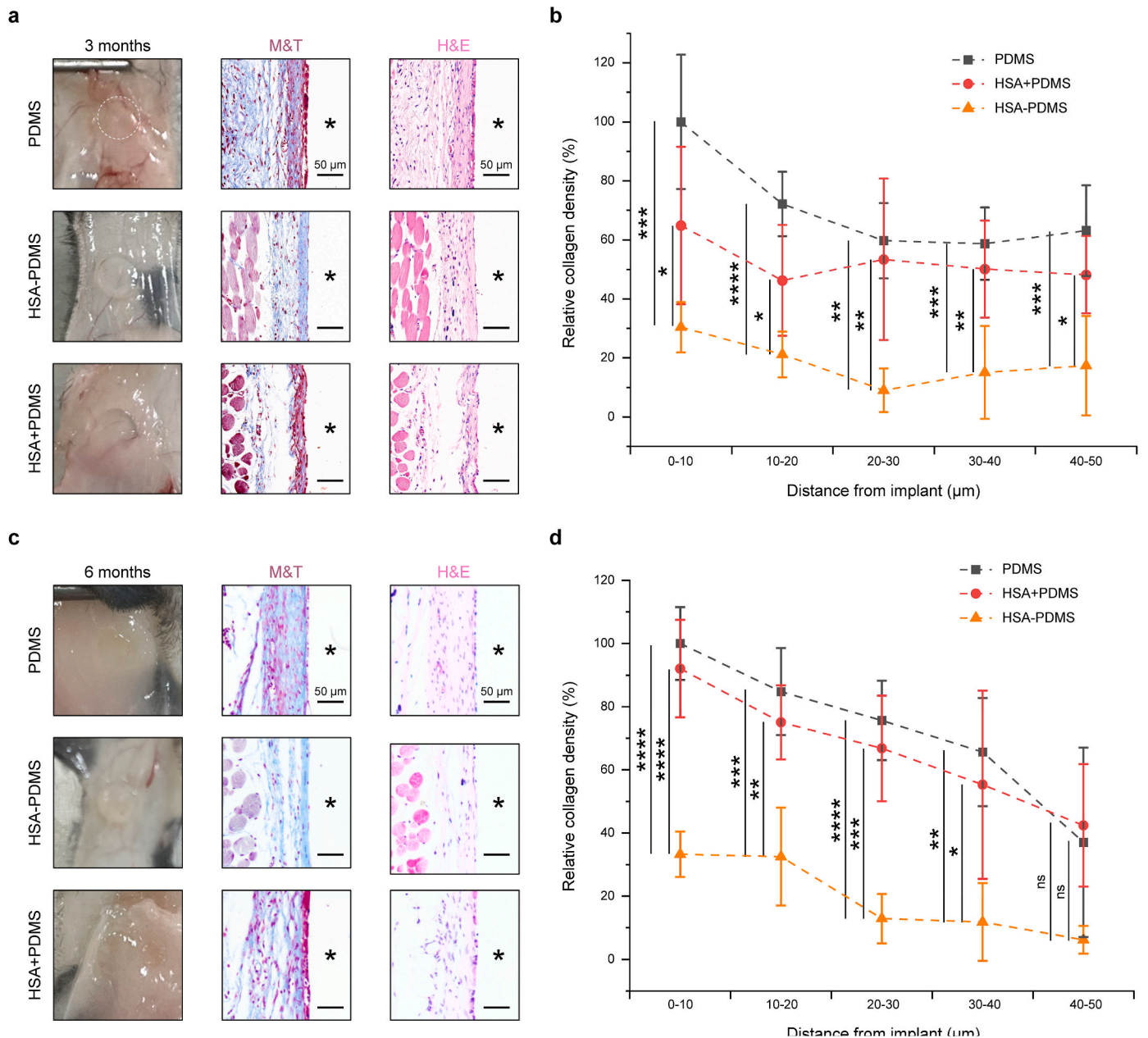


Fig. 6. Long-term FBR resistance of albumin-coated materials. **a,c**) Digital photos, H&E-, and M&T-stained histological sections of excised 3-month and 6-month post-implantation. The white dashed circle represents the PDMS disc that is not visible to the naked eye due to strong collagen capsule encapsulation after implantation. Asterisk sign "*" in the section images denote the original locations of the implants. **b,d**) Collagen capsule density 3-month and 6-month post-implantation measured by M&T staining ($n = 6$ mice per group, mean \pm s.d.). Statistical significance was determined by one-way analysis of variance (ANOVA) with Turkey post-test. * $P < 0.05$, ** $P < 0.01$, *** $P < 0.001$, **** $P < 0.0001$, ns: not significant. $P < 0.05$ is considered to have a significant difference.

experienced significant fibrosis, leading to the formation of a thick layer of collagen and complete invisibility by the third month. HSA+PDMS samples showed a certain inhibitory effect on fibrosis, but the results were not as effective as desired. The statistical results of collagen density show that compared to the uncoated PDMS group, HSA-PDMS can effectively reduce the collagen density at the material-tissue interface, which is ~30% and ~33% of the uncoated PDMS interface collagen density, while the HSA+PDMS group has an interface collagen density of ~65% and ~92% of uncoated PDMS after 3 and 6 months, respectively (Fig. 6b and d). The above results indicate that covalently grafted albumin coating can effectively mitigate the long-term fibrosis reaction of implants.

4. Conclusion

In summary, we have developed a facile and scalable albumin coating technique to overcome the challenge of foreign body response faced by implants. The results revealed that the stability of albumin coatings and the selection of albumin species sources are crucial for their long-term resistance to FBR. We compared the FBR effect of HSA-coated PDMS discs prepared by both physical adsorption and covalent bonding. Notably, physically adsorbed albumin coatings demonstrated alleviation in acute inflammation, while covalently grafted samples exhibited a dual capacity - easing acute inflammation and mitigating fibrosis over 6 months. We realized that the stable presence of albumin coating on the surface in the body environment is critical for resisting FBR, and subsequent *in vitro* protein displacement experiments confirmed that the albumin coating prepared through covalent grafting could effectively inhibit the displacement of other proteins, potentially contributing to their prolonged FBR resistance. Interestingly, we observed that HSA-coated samples were able to effectively inhibit FBR after implantation in mice. Considering the high homology of albumin from different mammals, we extended to test the FBR induced by albumin coating from other species. The results unveiled that solely HSA-coated samples effectively reduced FBR, although the underlying mechanism requires further research. Further studies might be focused on answering the question that why only human albumin coatings rather than albumins from other species alleviate the FBR in mouse models. It would be also important to evaluate the coating performance on other material substrates (e.g. ceramics and metals) and additional massive experimental validations are needed to confirm the clinical benefits of this coating on devices. The albumin coating method stands as a simple and effective approach for anti-FBR coatings across biomaterials for implants, potentially enhancing *in vivo* performance and reducing fibrosis-linked complications.

Competing interests

The authors declare no competing interests.

Ethics approval and consent to participate

All animal experiments are in compliance with the relevant regulations, and all protocols are approved by the Institutional Animal Care and Use Committee, Zhejiang Academy of Medical Sciences. Approval No. ZJCLA-IACUC-20010236.

CRediT authorship contribution statement

Xianchi Zhou: Writing – review & editing, Writing – original draft, Visualization, Validation, Software, Resources, Methodology, Investigation, Formal analysis, Data curation. **Hongye Hao:** Investigation. **Yifeng Chen:** Investigation. **Wenzhong Cao:** Investigation. **Zihao Zhu:** Investigation. **Yanwen Ni:** Software. **Zuolong Liu:** Software. **Fan Jia:** Validation. **Youxiang Wang:** Supervision. **Jian Ji:** Supervision. **Peng Zhang:** Writing – review & editing, Supervision, Project administration,

Funding acquisition, Conceptualization.

Acknowledgements

This work was supported by the National Key R&D Program of China (2022YFB3807300), the National Natural Science Foundation of China (52103188, 22175152), the Joint Funds of the Zhejiang Provincial Natural Science Foundation of China and Huadong Medicine (LHDMZ22H300011), the Fundamental Research Funds for the Central Universities (226-2022-00146), and the startup package of Zhejiang University.

Appendix A. Supplementary data

Supplementary data to this article can be found online at <https://doi.org/10.1016/j.bioactmat.2024.01.006>.

References

- [1] Y. Song, L. Li, W. Zhao, Y. Qian, L. Dong, Y. Fang, L. Yang, Y. Fan, Surface modification of electrospun fibers with mechano-growth factor for mitigating the foreign-body reaction, *Bioact. Mater.* 6 (2021) 2983–2998.
- [2] J.M. Anderson, A. Rodriguez, D.T. Chang, Foreign body reaction to biomaterials, *Semin. Immunol.* 20 (2008) 86–100.
- [3] D. Zhang, Q. Chen, C. Shi, M. Chen, K. Ma, J. Wan, R. Liu, Dealing with the foreign-body response to implanted biomaterials: strategies and applications of new materials, *Adv. Funct. Mater.* 31 (2020) 2007226.
- [4] Y. Chandorkar, R. K. B. Basu, The foreign body response demystified, *ACS Biomater. Sci. Eng.* 5 (2019) 19–44.
- [5] N. Kutner, K.R. Kunduru, L. Rizik, S. Farah, Recent advances for improving functionality, biocompatibility, and longevity of implantable medical devices and deliverable drug delivery systems, *Adv. Funct. Mater.* 31 (2021) 2010929.
- [6] O. Veisoh, A.J. Vegas, Domesticating the foreign body response: recent advances and applications, *Adv. Drug Deliv. Rev.* 144 (2019) 148–161.
- [7] L. Chung, D.R. Maestas, A. Lebid, A. Mageau, G.D. Rosson, X. Wu, M.T. Wolf, A. J. Tam, I. Vanderzee, X. Wang, Interleukin 17 and senescent cells regulate the foreign body response to synthetic material implants in mice and humans, *Sci. Transl. Med.* 12 (2020) eaax3799.
- [8] D. Zhang, Q. Chen, Y. Bi, H. Zhang, M. Chen, J. Wan, C. Shi, W. Zhang, J. Zhang, Z. Qiao, Bio-inspired poly-DL-serine materials resist the foreign-body response, *Nat. Commun.* 12 (2021) 1–12.
- [9] D. Zhang, Q. Chen, W. Zhang, H. Liu, J. Wan, Y. Qian, B. Li, S. Tang, Y. Liu, S. Chen, R. Liu, Silk-inspired beta-peptide materials resist fouling and the foreign-body response, *Angew. Chem. Int. Ed.* 59 (2020) 9586–9593.
- [10] J. Zhang, Y. Zhu, J. Song, J. Yang, C. Pan, T. Xu, L. Zhang, Novel balanced charged alginate/PEI polyelectrolyte hydrogel that resists foreign-body reaction, *ACS Appl. Mater. Interfaces* 10 (2018) 6879–6886.
- [11] D. Dong, C. Tsao, H.-C. Hung, F. Yao, C. Tang, L. Niu, J. Ma, J. MacArthur, A. Sinclair, K. Wu, High-strength and fibrous capsule-resistant zwitterionic elastomers, *Sci. Adv.* 7 (2021) eabc5442.
- [12] H. Wang, H. Li, Y. Wu, J. Yang, W. Liu, A high strength, anti-fouling, self-healable, and thermoplastic supramolecular polymer hydrogel with low fibrotic response, *Sci. China Technol. Sci.* 62 (2019) 569–577.
- [13] L. Zhang, Z. Cao, T. Bai, L. Carr, J.R. Ella-Menye, C. Irvin, B.D. Ratner, S. Jiang, Zwitterionic hydrogels implanted in mice resist the foreign-body reaction, *Nat. Biotechnol.* 31 (2013) 553–556.
- [14] S. Farah, J.C. Doloff, P. Muller, A. Sadraei, H.J. Han, K. Olafson, K. Vyas, H.H. Tam, J. Hollister-Lock, P.S. Kowalski, M. Griffin, A. Meng, M. McAvoy, A.C. Graham, J. McGarrigle, J. Oberholzer, G.C. Weir, D.L. Greiner, R. Langer, D.G. Anderson, Long-term implant fibrosis prevention in rodents and non-human primates using crystallized drug formulations, *Nat. Mater.* 18 (2019) 892–904.
- [15] T.T. Dang, K.M. Bratlie, S.R. Bogatyrev, X.Y. Chen, R. Langer, D.G. Anderson, Spatiotemporal effects of a controlled-release anti-inflammatory drug on the cellular dynamics of host response, *Biomaterials* 32 (2011) 4464–4470.
- [16] N.M. Vacanti, H. Cheng, P.S. Hill, J.D. Guerreiro, T.T. Dang, M. Ma, S. Watson, N. S. Hwang, R. Langer, D.G. Anderson, Localized delivery of dexamethasone from electrospun fibers reduces the foreign body response, *Biomacromolecules* 13 (2012) 3031–3038.
- [17] O. Veisoh, J.C. Doloff, M. Ma, A.J. Vegas, H.H. Tam, A.R. Bader, J. Li, E. Langan, J. Wyckoff, W.S. Loo, S. Jhunjunwala, A. Chiu, S. Siebert, K. Tang, J. Hollister-Lock, S. Aresta-Dasilva, M. Bochenek, J. Mendoza-Elias, Y. Wang, M. Qi, D. M. Lavin, M. Chen, N. Dholakia, R. Thakrar, I. Lacik, G.C. Weir, J. Oberholzer, D. L. Greiner, R. Langer, D.G. Anderson, Size- and shape-dependent foreign body immune response to materials implanted in rodents and non-human primates, *Nat. Mater.* 14 (2015) 643–651.
- [18] W.K. Ward, E.P. Slobodzian, K.L. Tiekotter, M.D. Wood, The effect of microgeometry, implant thickness and polyurethane chemistry on the foreign body response to subcutaneous implants, *Biomaterials* 23 (2002) 4185–4192.
- [19] J.C. Doloff, O. Veisoh, R. de Mezerville, M. Sforza, T.A. Perry, J. Haupt, M. Jamiel, C. Chambers, A. Nash, S. Aghlara-Fotovat, J.L. Stelzel, S.J. Bauer, S.Y. Neshat,

- J. Hancock, N.A. Romero, Y.E. Hidalgo, I.M. Leiva, A.M. Munhoz, A. Bayat, B. M. Kinney, H.C. Hodges, R.N. Miranda, M.W. Clemens, R. Langer, The surface topography of silicone breast implants mediates the foreign body response in mice, rabbits, and humans, *Nat. Biomed. Eng.* 5 (2021) 1115–1130.
- [20] E.M. Sussman, M.C. Halpin, J. Muster, R.T. Moon, B.D. Ratner, Porous implants modulate healing and induce shifts in local macrophage polarization in the foreign body reaction, *Ann. Biomed. Eng.* 42 (2014) 1508–1516.
- [21] L.E. Jansen, L.D. Amer, E.Y. Chen, T.V. Nguyen, L.S. Saleh, T. Emrick, W.F. Liu, S. J. Bryant, S.R. Peyton, Zwitterionic PEG-PC hydrogels modulate the foreign body response in a modulus-dependent manner, *Biomacromolecules* 19 (2018) 2880–2888.
- [22] N. Noskovicova, R. Schuster, S. van Putten, M. Ezzo, A. Koehler, S. Boo, N. M. Coelho, D. Griggs, P. Ruminski, C.A. McCulloch, B. Hinz, Suppression of the fibrotic encapsulation of silicone implants by inhibiting the mechanical activation of pro-fibrotic TGF-beta, *Nat. Biomed. Eng.* 5 (2021) 1437–1456.
- [23] S. Bose, L.R. Volpatti, D. Thiono, V. Yesilyurt, C. McGladrigan, Y. Tang, A. Facklam, A. Wang, S. Jhunjunwala, O. Veisheh, J. Hollister-Lock, C. Bhattacharya, G.C. Weir, D.L. Greiner, R. Langer, D.G. Anderson, A retrievable implant for the long-term encapsulation and survival of therapeutic xenogeneic cells, *Nat. Biomed. Eng.* 4 (2020) 814–826.
- [24] S. J. Karinja, J. L. Bernstein, S. Mukherjee, J. Jin, A. Lin, A. Abadeer, O. Kaymakcalan, O. Veisheh, J. A. Spector, An anti-fibrotic breast implant surface coating significantly reduces peri-prosthetic capsule formation, *Plast. Reconstr. Surg.* e010323...
- [25] A.J. Vegas, O. Veisheh, J.C. Doloff, M. Ma, H.H. Tam, K. Bratlie, J. Li, A.R. Bader, E. Langan, K. Olejnik, P. Fenton, J.W. Kang, J. Hollister-Locke, M.A. Bochenek, A. Chiu, S. Siebert, K. Tang, S. Jhunjunwala, S. Aresta-Dasilva, N. Dholakia, R. Thakrar, T. Vietti, M. Chen, J. Cohen, K. Siniakowicz, M. Qi, J. McGarrigle, A. C. Graham, S. Lyle, D.M. Harlan, D.L. Greiner, J. Oberholzer, G.C. Weir, R. Langer, D.G. Anderson, Combinatorial hydrogel library enables identification of materials that mitigate the foreign body response in primates, *Nat. Biotechnol.* 34 (2016) 345–352.
- [26] Q. Li, C. Wen, J. Yang, X. Zhou, Y. Zhu, J. Zheng, G. Cheng, J. Bai, T. Xu, J. Ji, S. Jiang, L. Zhang, P. Zhang, Zwitterionic biomaterials, *Chem. Rev.* 122 (2022) 17073–17154.
- [27] Y.K. Kim, R. Que, S.W. Wang, W.F. Liu, Modification of biomaterials with a self-protein inhibits the macrophage response, *Adv. Healthcare Mater.* 3 (2014) 989–994.
- [28] S.J. Stachelek, M.J. Finley, I.S. Alferiev, F. Wang, R.K. Tsai, E.C. Eckells, N. Tomczyk, J.M. Connolly, D.E. Discher, D.M. Eckmann, R.J. Levy, The effect of CD47 modified polymer surfaces on inflammatory cell attachment and activation, *Biomaterials* 32 (2011) 4317–4326.
- [29] H. Yan, M. Melin, K. Jiang, M. Trossbach, B. Badadmath, K. Langer, B. Winkeljann, O. Lieleleg, J. Hong, H.N. Joensson, T. Crouzier, Immune-modulating mucin hydrogel microdroplets for the encapsulation of cell and microtissue, *Adv. Funct. Mater.* 31 (2021) 2105967.
- [30] H. Yan, M. Hjorth, B. Winkeljann, I. Dobryden, O. Lieleleg, T. Crouzier, Glyco-modification of mucin hydrogels to investigate their immune activity, *ACS Appl. Mater. Interfaces* 12 (2020) 19324–19336.
- [31] H. Yan, C. Seigne, M. Hjorth, B. Winkeljann, M. Blakeley, O. Lieleleg, M. Phillipson, T. Crouzier, Immune-informed mucin hydrogels evade fibrotic foreign body response in vivo, *Adv. Funct. Mater.* 29 (2019) 1902581.
- [32] K. Zhang, H. Huang, H.-C. Hung, C. Leng, S. Wei, R. Crisci, S. Jiang, Z. Chen, Strong hydration at the poly(ethylene glycol) brush/albumin solution interface, *Langmuir* 36 (2020) 2030–2036.
- [33] J. Ouyang, Q. Bu, N. Tao, M. Chen, H. Liu, J. Zhou, J. Liu, B. Deng, N. Kong, X. Zhang, T. Chen, Y. Cao, W. Tao, A facile and general method for synthesis of antibiotic-free protein-based hydrogel: wound dressing for the eradication of drug-resistant bacteria and biofilms, *Bioact. Mater.* 18 (2022) 446–458.
- [34] X. Gao, Z. Han, C. Huang, H. Lei, G. Li, L. Chen, D. Feng, Z. Zhou, Q. Shi, L. Cheng, X. Zhou, An anti-inflammatory and neuroprotective biomimetic nanopatform for repairing spinal cord injury, *Bioact. Mater.* 18 (2022) 569–582.
- [35] Z. Liu, X. Zhou, Y. Chen, Y. Ni, Z. Zhu, W. Cao, K. Chen, Y. Yan, J. Ji, P. Zhang, Fibrous capsule-resistant, controllable degradable and functionalizable zwitterion-albumin hybrid hydrogels, *Biomater. Sci.* DOI: 10.1039/D3BM01783D...
- [36] S. Hussain, Z. Babar, J. Hadid, J. McLaughlin, Coating polyurethane with palmitoleic acid and bovine serum albumin to prevent the host response to foreign materials, *Am. J. Undergrad. Res.* 16 (2020) 5–13.
- [37] C. Tao, W. Zhu, J. Iqbal, C. Xu, D.A. Wang, Stabilized albumin coatings on engineered xenografts for attenuation of acute immune and inflammatory responses, *J. Mater. Chem. B* 8 (2020) 6080–6091.
- [38] X. Hu, J. Tian, C. Li, H. Su, R. Qin, Y. Wang, X. Cao, P. Yang, Amyloid-like protein aggregates: a new class of bioinspired materials merging an interfacial anchor with antifouling, *Adv. Mater.* 32 (2020) 2000128.
- [39] S.Y. Jung, S.M. Lim, F. Albertorio, G. Kim, M.C. Gurau, R.D. Yang, M.A. Holden, P. S. Cremer, The Vroman effect: a molecular level description of fibrinogen displacement, *J. Am. Chem. Soc.* 125 (2003) 12782–12786.
- [40] J.C. Doloff, O. Veisheh, A.J. Vegas, H.H. Tam, S. Farah, M. Ma, J. Li, A. Bader, A. Chiu, A. Sadraei, S. Aresta-Dasilva, M. Griffin, S. Jhunjunwala, M. Webber, S. Siebert, K. Tang, M. Chen, E. Langan, N. Dholakia, R. Thakrar, M. Qi, J. Oberholzer, D.L. Greiner, R. Langer, Colony stimulating factor-1 receptor is a central component of the foreign body response to biomaterial implants in rodents and non-human primates, *Nat. Mater.* 16 (2017) 671–680.
- [41] A. Abuchowski, T. van Es, N.C. Palczuk, F.F. Davis, Alteration of immunological properties of bovine serum albumin by covalent attachment of polyethylene glycol, *J. Biol. Chem.* 252 (1977) 3578–3581.
- [42] S. Spitzauer, C. Schweiger, W.R. Sperr, B. Pandjaitan, P. Valent, S. Mühl, C. Ebner, O. Scheiner, D. Kraft, H. Rumpold, R. Valenta, Molecular characterization of dog albumin as a cross-reactive allergen, *J. Allergy Clin. Immunol.* 93 (1994) 617–627.